JOURNAL OF GEOPHYSICAL RESEARCH, VOL. 113, D16S46, doi:10.1029/2007JD008808, 2008

The 2005 and 2006 DANDELIONS NO_2 and aerosol intercomparison campaigns

E. J. Brinksma,[1] G. Pinardi,[2] H. Volten,[1,3] R. Braak,[1] A. Richter,[4] A. Schönhardt,[4] M. van Roozendael,[2] C. Fayt,[2] C. Hermans,[2] R. J. Dirksen,[1] T. Vlemmix,[1] A. J. C. Berkhout,[3] D. P. J. Swart,[3] H. Oetjen,[4] F. Wittrock,[4] T. Wagner,[5,6] O. W. Ibrahim,[6] G. de Leeuw,[7,8,9] M. Moerman,[7] R. L. Curier,[7] E. A. Celarier,[10] A. Cede,[11] W. H. Knap,[1] J. P. Veefkind,[1] H. J. Eskes,[1] M. Allaart,[1] R. Rothe,[1] A. J. M. Piters,[1] and P. F. Levelt[1]

Received 14 April 2007; revised 14 January 2008; accepted 21 February 2008; published 25 July 2008.

[1] Dutch Aerosol and Nitrogen Dioxide Experiments for Validation of OMI and SCIAMACHY (DANDELIONS) is a project that encompasses validation of spaceborne measurements of NO_2 by the Ozone Monitoring Instrument (OMI) and Scanning Imaging Absorption Spectrometer for Atmospheric Cartography (SCIAMACHY), and of aerosol by OMI and Advanced Along-Track Scanning Radiometer (AATSR), using an extensive set of ground-based and balloon measurements over the polluted area of the Netherlands. We present an extensive data set of ground-based, balloon, and satellite data on NO_2, aerosols, and ozone obtained from two campaigns within the project, held during May–June 2005 and September 2006. We have used these data for first validation of OMI NO_2, and the data are available through the Aura Validation Data Center website for use in other validation efforts. In this paper we describe the available data, and the methods and instruments used, including the National Institute of Public Health and the Environment (RIVM) NO_2 lidar. We show that NO_2 from Multi-Axis Differential Optical Absorption Spectroscopy (MAX-DOAS) compares well with in situ measurements. We show that different MAX-DOAS instruments, operating simultaneously during the campaign, give very similar results. We also provide unique information on the spatial homogeneity and the vertical and temporal variability of NO_2, showing that during a number of days, the NO_2 columns derived from measurements in different directions varied significantly, which implies that, under polluted conditions, measurements in one single azimuth direction are not always representative for the averaged field that the satellite observes. In addition, we show that there is good agreement between tropospheric NO_2 from OMI and MAX-DOAS, and also between total NO_2 from OMI and direct-sun observations. Observations of the aerosol optical thickness (AOT) show that values derived with three ground-based instruments correspond well with each other, and with aerosol optical thicknesses observed by OMI.

Citation: Brinksma, E. J., et al. (2008), The 2005 and 2006 DANDELIONS NO_2 and aerosol intercomparison campaigns, *J. Geophys. Res.*, *113*, D16S46, doi:10.1029/2007JD008808.

1. Introduction

[2] Satellite data on NO_2 and aerosols provide important information on the spatial and temporal variability of air quality to the scientific community, which in turn feeds the information forward to policy and decision makers. The quality and reliability of these parameters is, therefore, important and dependent on adequate validation by independent sources. Validation campaigns advance the state of knowledge in the retrieval of remotely sensed parameters.

[3] DANDELIONS (Dutch Aerosol and Nitrogen Dioxide Experiments for Validation of OMI and SCIAMACHY)

[1]Climate Research and Seismology Department, Royal Netherlands Meteorological Institute, De Bilt, Netherlands.
[2]Belgian Institute for Space Aeronomy, Brussels, Belgium.
[3]Netherlands National Institute for Public Health and the Environment, Bilthoven, Netherlands.
[4]Institute of Environmental Physics, University of Bremen, Bremen, Germany.
[5]Max-Planck-Institute for Chemistry, Mainz, Germany.
[6]Institute for Environmental Physics, Heidelberg University, Heidelberg, Germany.
[7]TNO Defense, Security and Safety, The Hague, Netherlands.
[8]R&D, Climate Change Unit, Finnish Meteorological Institute, Helsinki, Finland.
[9]Department of Physical Sciences, University of Helsinki, Helsinki, Finland.
[10]SGT, Inc., Greenbelt, Maryland, USA.
[11]NASA Goddard Space Flight Center, Greenbelt, Maryland, USA.

0148-0227/08/2007JD008808$09.00

is a project that encompasses validation of NO_2 measurements by the Ozone Monitoring Instrument (OMI) and SCIAMACHY (Scanning Imaging Absorption Spectrometer for Atmospheric Cartography), and of aerosol measurements by OMI and the Advanced Along-Track Scanning Radiometer (AATSR), using an extensive set of ground-based and balloon measurements over the Netherlands, which is almost always polluted.

[4] Validation measurements were performed during two campaigns at the Cabauw Experimental Site for Atmospheric Research (CESAR, 51.97°N, 4.93°E, 0.70 m below mean sea level) [*Russchenberg et al.*, 2005] which ran from 8 May through 14 July 2005 and 1–30 September 2006, respectively. We present an extensive data set of ground-based, balloon and satellite data on total and tropospheric NO_2, aerosol optical thickness, and total and tropospheric ozone, which is available for validation of Aura instruments through the Aura Validation Data Center (AVDC). The DANDELIONS campaigns provide a unique opportunity to study the quality of DOAS-type measurements, with an unprecedented number of six Multi-Axis Differential Optical Absorption Spectroscopy (MAX-DOAS) instruments simultaneously retrieving NO_2 in addition to in situ NO_2 monitors and an NO_2 lidar.

[5] An important input to satellite NO_2 column retrieval is the assumed vertical distribution of NO_2, which is used in airmass factor calculations, since the profile shape directly influences the conversion from slant column to total NO_2. For thorough validation in polluted areas, measurements of the NO_2 profiles are therefore required [*Celarier et al.*, 2008]. There are only very few measurements of tropospheric NO_2 profiles available. The first results of a novel instrument, namely the NO_2 lidar developed at RIVM, that is able to measure lower tropospheric profiles are presented in this paper. We show that profiles compare well with in situ values near the surface and at 200 m. Although there are no profile measurements to validate the lidar against, the two-point comparisons with in situ and qualitative comparisons to MAX-DOAS, give confidence that the overall NO_2 lidar profiles, that range from near surface level up to 2500 m, are reliable.

[6] We show that the data contain unique information on the spatial homogeneity and the vertical and temporal variability of NO_2. We limit the analysis to the NO_2 and aerosol data collected, but we do provide an overview of the ozone data available from the campaigns at AVDC.

2. Satellite Retrieval Descriptions

2.1. Nitrogen Dioxide Algorithms

[7] The Ozone Monitoring Instrument (OMI) is a Dutch-Finnish instrument on board EOS-Aura, that has been in space since 15 July 2004 [*Levelt et al.*, 2006]. The operational OMI algorithm for total and tropospheric nitrogen dioxide [*Bucsela et al.*, 2006; *Boersma et al.*, 2002] proceeds in three steps. The first step is the retrieval of slant columns for NO_2 using the differential optical absorption spectroscopy (DOAS) method in the 405–465 nm range. To proceed further, an initial estimate of the vertical column density (vcd) is made using an airmass factor that is computed using an NO_2 profile shape representative for an unpolluted situation. OMI NO_2 slant columns, after correction for spurious across-track variability ('stripes') show a random error for individual pixels of approximately 1.1×10^{15} molec cm^{-2}.

[8] In the second step, various airmass factors are computed, on the basis of assumed NO_2 profile shapes for polluted and unpolluted scenes, and for clear and cloudy conditions.

[9] In the third step, data are assembled from each orbit and the orbits occurring within ±12 hours of it. Within 1° latitude bands a wave analysis (up to wave-2) is performed on the initial vertical columns after correcting for known persistent strong NO_2 sources, as well as any algorithmically determined outliers. The resulting model is then taken to represent the unpolluted field. If the initially retrieved vcd significantly exceeds this field, then the vcd is recomputed using an airmass factor computed assuming an NO_2 profile that had substantial tropospheric concentration. For details, we refer to the OMI NO_2 validation overview paper [*Celarier et al.*, 2008].

[10] Cloud fraction and cloud pressure are provided by a new cloud retrieval algorithm that uses the absorption of the O_2–O_2 collision complex near 477 nm [*Acarreta et al.*, 2004]. Tropospheric NO_2 retrievals are very sensitive to clouds; the consistency of cloud fraction and cloud pressure from the new O_2–O_2 (OMI) algorithm and from the Fast Retrieval Scheme for Cloud Observables (FRESCO) has been evaluated [*Boersma et al.*, 2006]. This showed that cloud parameters from the O_2–O_2 (OMI) algorithm had similar frequency distributions as cloud parameters retrieved from FRESCO (SCIAMACHY) for August 2006.

[11] These operational NO_2 data are referred to as OMI-L2 in this paper. Details on the computation can be found in the overview of validation efforts for OMI-L2 [*Celarier et al.*, 2008].

[12] The current paper also considers the Level 4 data (hereinafter, OMI-L4) [*Boersma et al.*, 2006]. OMI-L4 is generated from the OMI-L2 slant columns, with almost identical O_2–O_2 cloud information, but differ in the derivation of tropospheric NO_2 vertical columns, for which the combined retrieval-assimilation-modeling approach for offline tropospheric NO_2 developed at KNMI is used. The algorithm is very similar to the TEMIS algorithm applied for SCIAMACHY. In OMI-L4 the stratospheric contribution to the slant columns and the NO_2 profiles are calculated by running the TM4 chemistry transport model forward in time on the basis of forecast ECMWF meteorology and assimilated NO_2 information from all previous orbits. Tropospheric NO_2 slant columns are derived by subtracting the assimilated stratospheric slant column from the retrieved total slant column. They are subsequently divided by the tropospheric airmass factor, yielding tropospheric columns. The tropospheric airmass factor depends on viewing geometry, cloud coverage, cloud height, surface albedo and the NO_2 profile shape, and is taken from a look up table based on radiative transfer calculations that include a modeled a priori NO_2 profile shape.

[13] The NO_2 slant columns are calculated using a not yet released version of the retrieval algorithm, which in principle is identical to that of *Boersma et al.* [2006], but incorporates reprocessed OMI O_2–O_2 cloud data. The software versions of the retrieval algorithms used for OMI-L4 in this paper are listed in Table 1.

Table 1. Software Versions of the OMI-L4 Retrieval Algorithms Used in This Study

Product	Product Name	Version Number	Version Date
Clouds	OMCLDO2	1.01	15 May 2006
NO_2 slant column	OMNO2A	0.9	15 May 2006
Tropospheric NO_2 column	-	0.9.3.1	26 January 2006

[14] The SCIAMACHY instrument is a German-Dutch-Belgian instrument on board Envisat, that was launched in early 2002. Tropospheric NO_2 columns have been retrieved from SCIAMACHY measurements using various algorithms. In this paper, we only show one single SCIAMACHY data point, derived using the data product from BIRA-KNMI [*Boersma et al.*, 2004]. A more elaborate study also involving the University of Bremen tropospheric NO_2 product [*Richter et al.*, 2005] is planned (G. Pinardi et al., manuscript in preparation, 2008). Cloud fraction and cloud top height for SCIAMACHY are derived from the FRESCO algorithm [*Koelemeijer et al.*, 2003]. The TEMIS tropospheric NO_2 product [*Blond et al.*, 2006; *van der A et al.*, 2006] is the result of a collaboration between ESA-DUE, BIRA-IASB and KNMI, in the context of the TEMIS project. It is available from the TEMIS web page (www.temis.nl). BIRA provides the NO_2 slant columns, and KNMI performs the transformation into tropospheric vertical columns, using a retrieval similar to the OMI-L4 algorithm.

2.2. OMI Multiwavelength Aerosol Algorithm

[15] Aerosol extinction optical thickness (AOT) and NO_2 concentrations are both important parameters in studies of air quality. In addition, AOT measurements provide validation opportunities in their own right: During the campaign, AOT values derived from OMI observations have been compared with various ground-based measurements (see section 3.4 for more details).

[16] The OMI aerosol product presented in this paper is derived with the multiwavelength algorithm, OMAERO. We do not discuss results from the other OMI aerosol algorithm, which was developed by *Torres et al.* [2002]. This algorithm uses up to nineteen wavelength bands between 330 and 500 nm. All wavelength bands are essentially free of absorption and Raman features, except the 477 nm band which comprises an absorption feature of the O_2-O_2 collision complex and makes the algorithm sensitive to aerosol layer altitude. The multiwavelength algorithm uses fifty aerosol models that are defined by the size distribution, the complex refractive index, and the aerosol layer altitude. They represent the major aerosol types: desert dust, biomass burning, volcanic, and weakly absorbing aerosol. The OMAERO algorithm is restricted to cloud-free scenes, since only Rayleigh scattering and scattering by the mentioned aerosol types are considered, but no clouds.

[17] For an observed cloud-free scene, a best fit AOT at a certain reference wavelength is derived for each of the fifty aerosol models. This is achieved by minimizing a merit function that expresses the difference between the observed spectrum and a synthetic spectrum calculated using radiative transfer code that includes multiple scattering and polarization, and checking that the aerosol model is allowed according to a geographical aerosol climatology. Over the Netherlands, the climatology only allows weakly absorbing aerosols. AOT values at other wavelengths are readily calculated using the single-scattering properties of the relevant aerosol model.

[18] The retrieved AOT is sensitive to the surface albedo spectrum. In the current implementation of the OMAERO algorithm, a monthly climatology based on MISR (Multiangle Imaging SpectroRadiometer) data is used over land, and a computational model based on wind and chlorophyll climatologies is used over oceans. The true surface albedo may deviate significantly from the climatology in certain circumstances, although this is not expected to be a major issue for the Cabauw site as opposed to sites at higher

Table 2. Overview of Instrumentation During the DANDELIONS-2 Campaign

Instrument	Group	Data
OMI	KNMI/NASA	NO_2 columns: level 2 & level 4, AOT
SCIAMACHY	KNMI	NO_2 columns: TEMIS and Bremen
AATSR	KNMI	aerosol type, AOT, Ångström coefficient
NO_2 lidar	RIVM	NO_2 profiles 0–2.5 km
NO_2 monitor	RIVM	NO_2 surface concentrations
NO_2 monitor[a,b]	RIVM	NO_2 concentrations at 200 m
Boundary layer lidar	RIVM	aerosol extinction, backscatter profiles
MAX DOAS	IUP Bremen	NO_2 columns, profiles 0–2.5 km
MAX DOAS	IUP Heidelberg	NO_2 columns, three azimuth angles
MAX DOAS	BIRA Brussels	NO_2 columns
Direct-sun DOAS[b]	BIRA Brussels	NO_2 columns
Mini MAX DOAS[a]	BIRA Brussels	NO_2 columns
Mini MAX DOAS	KNMI	NO_2 columns
Radiosondes	KNMI	pressure, temperature, RH
Ozone sondes[c]	KNMI	ozone profiles
Brewer spectrophotometer[c]	KNMI	ozone columns
GLOBE spectrophotometer	KNMI	AOT
Pandora direct-sun spectrometer	NASA/GSFC[b]	NO_2
Routine aerosol instruments	TNO/KNMI	AOT

[a]Placed in the tower at 200 m height.
[b]Participated only during the 2006 campaign.
[c]Ozone launches and Brewer from location De Bilt.

Table 3. DOAS Instrument Details

	BIRA MAX-DOAS Surface	BIRA MiniDOAS 200 m	BIRA MAX-DOAS Surface	BIRA Direct-Sun Surface	Heidelberg MAX-DOAS Surface	Bremen MAX-DOAS Surface (VIS)	Bremen MAX-DOAS Surface (VIS)	Bremen MAX-DOAS Surface (UV)
Period	3 May to 19 July 2005	1 Sept to 2 Oct 2006	8 Sept to 2 Oct 2006	6–26 Sept 2006	2005 and 2006	2005	2006	2006
Spectrometer	ORIEL MS127	OceanOptics USB2000	ORIEL MS127	ARC SP2150		ARC 500	ARC 275	ARC 500
Detectors	PI CCD	Sony ILX511 CCD	PI CCD	PI CCD	CCD	PI CCD	PI CCD	PI CCD
	400 × 1340 pixels	2048 pixels	100 × 1340 pixels	400 × 1340 pixels	256 × 1024 pixels	1340 × 400 pixels	1340 × 100 pixels	1340 × 400 pixels
Detector T	233 K	263 K	228 K	228 K	245 K	243 K	243 K	243 K
Grating	1200 grooves/mm	2400 grooves/mm	1200 grooves/mm	1200 grooves/mm	1200 grooves/mm	300 grooves/mm	300 grooves/mm	600 grooves/mm
	blazed at 300 nm		blazed at 240 nm	blazed at 300 nm	blazed at ..nm	blazed at 300 nm	blazed at 500 nm	blazed at 300 nm
Resolution FWHM	0.55 nm	0.6 nm	0.7 nm	0.56 nm	0.75 nm	0.6 nm	1 nm	0.4 nm
Wavelengths	308–455 nm	290–435 nm	322–467 nm	335–450 nm	320–457 nm	331–503 nm	400–714 nm	325–408 nm
Azimuth direction	S	S	S	S	298° (WNW), 208° (SSW), 118° (ESE)	234°	234°	234°
Field-of-View	6°	0.6°	1°	4°	0.8°	1°	1°	1°
Viewing geometry	0–15[a], 30, 90	−10–−4,[b] −3–+7[a] 8–16,[b] 20, 25, 30, 90	0–6, [a]8–16[b] 20, 25, 30, 90	Sun-tracking	1, 3, 6, 10, 30, 90	0–15, [a]30, 90	0–16[b], 30, 90	0–16, [b]30, 90

[a]In 1° steps.
[b]In 2° steps.

latitudes. For the Cabauw location in September, at 500 nm a value of 0.044 is used. The surface reflectivity and its wavelength dependence were accurately determined from OMI and AERONET data, and were used in an updated version of OMAERO as described by *Curier et al.* [2008]. More information on the OMAERO aerosol algorithm is available elsewhere [*Stammes,* 2002; *Torres et al.*, 2007].

3. Ground-Based and Balloon Instrument Descriptions

[19] An overview of instruments participating in the 2005 and 2006 campaigns is presented in Table 2. In addition, the Cabauw site has a large number of routine instruments aimed at measuring meteorological, radiative and cloud parameters [*Russchenberg et al.*, 2005]. We describe first the instruments primarily measuring NO_2, then instruments primarily measuring aerosols, and then the additional suite of instrumentation.

3.1. DOAS Instruments and Retrievals

[20] During the DANDELIONS campaigns, three Multi-Axis Differential Optical Absorption Spectroscopy (MAX-DOAS) instruments operated quasi-continuously in Cabauw, namely the MAX-DOAS instruments of BIRA-IASB, University of Bremen and IUP Heidelberg. Operational details are summarized in Table 3. In addition to these instruments, two commercial mini-MAX-DOAS systems from Hoffmann Messtechnik GmbH were operated, namely the BIRA-IASB MiniDOAS, which operated successfully from the top of the tower during the 2006 campaign, and the KNMI MiniDOAS, which was tested during 2005, and operated successfully from the surface near the tower base in 2006. All MAX-DOAS instruments measured throughout the day, using nighttime for calibrations.

[21] During the second campaign, BIRA operated an additional direct-sun DOAS instrument. These measurements are characterized by a well-defined optical path and therefore provide accurate NO_2 total columns. The Pandora instrument yielded only a limited amount of NO_2 results at the very end of DANDELIONS-2, owing to technical problems.

3.1.1. Generic Description of DOAS Instruments

[22] A Multi-Axis DOAS (MAX-DOAS) instrument typically consists of two main parts: a grating spectrometer with a linear or two-dimensional detector mounted inside a thermoregulated box that is located inside a building, and one or more scanning telescopes connected to the spectrometer via fiber optics. We present a generic description of the instruments and their retrieval methods here, while specific details are summarized in Table 4. MAX-DOAS instruments and retrievals have been described in more detail elsewhere [*Sinreich et al.*, 2005; *Honninger et al.*, 2004; *Wittrock et al.*, 2004].

[23] The telescopes sequentially collect scattered sun light at various elevation angles, in one fixed azimuthal direction per telescope. In the box, a grating spectrometer disperses the light with wavelength ranges varying for the different instruments as specified in Table 4. The signals are recorded by cooled CCD arrays and stored on personal computers.

[24] Consecutive measurements at increasing elevation angles are performed, forming an acquisition cycle, which

Table 4. DOAS Retrieval Details

	Bremen VIS (2005 and 2006)	Bremen UV (2006)	Heidelberg	BIRA MAX-DOAS and Direct Sun	BIRA MiniDOAS
Fit window 1	450–497 nm	344.7–370 nm	415–445 nm	425–450 nm	407–432 nm
Polynomial order	3	4	3	2 (5 for direct sun)	2
O_3	241 K	221 K and 241 K	243 K	223 K	223 K
NO_2	220 K	293 K	294 K	220 K	220 K
NO_2	294–220 K	–	–	295–221 K	295–221 K
O_2–O_2	296 K	296 K	–	yes	yes
BrO	–	228 K	–	–	–
H_2O	yes	–	yes	yes	yes
Ring	yes	yes	yes	yes	yes

always contains a number of elevations close to the horizontal, and a zenith observation. The horizon pointing measurements have a large sensitivity to absorptions in the boundary layer while the zenith measurements are used as background spectra to account for Fraunhofer structures and stratospheric absorption. Close to sunrise and sunset, these cycles are replaced by zenith observations only, to enable classical DOAS twilight retrievals which focus on stratospheric retrievals.

[25] As a typical example, the BIRA-IASB group uses an acquisition cycle of successive integrations of about one minute duration from horizon up to 15° elevation, in 1° steps, followed by one measurement at 30° and one at zenith. Such a cycle takes about 30 minutes. At solar zenith angles larger than 85°, the multi-axis cycle is replaced by continuous zenith sky measurements.

[26] The Heidelberg MAX-DOAS instrument differs from the others in that it has a set of three moveable telescopes, which enable simultaneous measurement cycles in three azimuth viewing directions. The individual quartz fibers from each bundle associated with the three different telescopes are arranged in a vertical column at the entrance slit of the spectrograph (with two gaps between the three fiber bundles [see *Wagner et al.*, 2004]).

[27] For the Bremen instrument [*Wittrock et al.*, 2004], the zenith direction is viewed without a mirror, while the other elevation angles in the measurement cycle are selected through a rotating mirror inside the telescope. The range of angles is 0–30° with respect to the horizontal. While in 2005 the Bremen group operated only one instrument, for which the NO_2 retrieval was performed in the visible wavelength region, two instruments were set up in 2006, one for the visible and one for the ultraviolet wavelengths.

[28] For the BIRA MAX-DOAS instrument, the elevation angles were scanned using a movable telescope for 2005, while in 2006 a rotating mirror before the telescope was used to select the viewing angle. The acquisition parameters of the MiniDOAS instruments were similar to those of the ground instrument (same viewing direction, and similar cycle of elevation angle scan) with the exception that the MiniDOAS on top of the tower was also allowed to scan negative elevation angles.

[29] The BIRA direct-sun DOAS instrument is similar in concept to the MAX-DOAS: inside the building, in a thermoregulated box, a grating spectrometer covering the UV-VIS region coupled to a cooled CCD detector, connected by depolarizing fiber optic bundle to an external optical head. The latter is a collimating optic tube limiting the field-of-view, mounted on a BRUSAG commercial sun-tracking system, holding the fiber.

3.1.2. Generic Description of DOAS Retrievals

[30] Scattered light sky spectra are analyzed using the well-known Differential Optical Absorption Spectroscopy (DOAS) technique [*Noxon*, 1975; *Platt*, 1994]. The fitting window used for NO_2 is specified in Table 4. In the second campaign, the Bremen group operated separate instruments for the UV and VIS, and hence also used two fitting windows, also specified in Table 4.

[31] Besides NO_2, a number of other absorbers, plus the Ring effect, are taken into account in the fit, which also includes a polynomial and an additive polynomial for straylight correction. In order to account for the temperature dependence of the NO_2 absorption spectrum, a second cross section (difference between 295 K and 221 K) may be introduced in the retrieval to improve the fit and correct the vertical column derived. In addition, this potentially allows derivation of the effective air temperature at the bulk of the NO_2 profile. It should be noted that currently not all retrievals used NO_2 cross sections at two temperatures, and thus systematic differences are expected to arise. Since the wavelength positions of the absorption cross sections are fixed, the measured scattered light spectra are calibrated by alignment on a high-resolution solar spectrum [*Kurucz et al.*, 1984].

[32] Evaluation of the stratospheric and tropospheric columns of NO_2 has been performed for all MAX-DOAS observations. Stratospheric columns are derived from late twilight zenith-sky measurements (SZA larger than 90°) when the sensitivity to the troposphere is minimal, while tropospheric columns are retrieved from tropospheric differential slant columns ($SCD_{off\text{-}axis} - SCD_{zenith}$) at 15° and 30° of elevation. The conversion into tropospheric vertical columns is obtained using simple geometrical considerations assuming that the NO_2 layer is located below the scattering altitude, using the following equation:

$$vcd_{trop} = \frac{SCD_{off\ axis} - SCD_{zenith}}{\sin^{-1}(los) - 1}. \quad (1)$$

The approach is based on two assumptions: first, that the stratospheric absorption is similar in the horizon-viewing and zenith-sky direction and therefore cancels, and second, that for 15° and 30° viewing angle, the geometric light path enhancement is a good approximation in the boundary layer. The results from the 30° and 15° directions are compared

Table 5. Altitude Ranges for Different Elevation Angles Used in the NO_2 Lidar Measurement Sequence, Assuming a Range Interval From 300 m to 2500 m, and Best Resolutions for an Accuracy Better Than 0.4 $\mu g/m^3$ Assuming a Range Interval of 450 m[a]

Elevation, deg	Altitude Interval, m	Best Resolution, m
0.75	4–33	6
1.5	8–65	12
3	16–131	24
6	31–261	47
12	62–520	94
24	122–1017	183
90	300–2500	450

[a]Altitude range and resolution depend also on atmospheric conditions.

and only those measurements where the results agree within 10% are retained. This approach ensures that the geometrical approximation used for the retrieval holds, and also eliminates measurement points strongly affected by clouds or horizontal inhomogeneities.

3.2. NO_2 Lidar

[33] NO_2 profiles were measured by a lidar system developed at RIVM [*Berkhout et al.*, 2006] which during the campaign was located about 200 m from the mast, only a few meters from the Heidelberg and Bremen MAX-DOAS instruments. The lidar consists of an emitter and a receiver unit. The entire system is housed in a truck, constituting a fully self-supporting mobile laboratory. Lidar descriptions in this paper refer exclusively to the 2006 configuration, which was significantly improved with respect to 2005.

[34] The emitter unit consists of a pulsed pump laser–dye laser combination, running at 30 Hz. The dye laser is tuned to 449.10 nm and detuned to 448.31 nm every other pulse. The latter wavelength undergoes absorption more strongly by NO_2 than the former. The laser pulses, 40 mJ in energy, 10 ns in duration, are directed into the atmosphere, where they are scattered by gas molecules and aerosol particles. The receiver unit collects the backscattered light using a 280 mm telescope on a photomultiplier tube, with an interference filter to block daylight; its passband is centered at 449.1 nm and is 3.35 nm wide. A digitizer samples the signals with a range resolution of 3.75 m.

[35] The NO_2 concentration over a certain altitude range is derived from the first derivative of the log of the ratio of the backscattered signals at the two wavelengths, using the differential absorption lidar (DIAL) method. The first derivative is determined over a number of 3.75 m range intervals; the number of intervals depends on the observed signal-to-noise of the signal ratio, and this determines the altitude resolution of the NO_2 profile. Typical resolutions are given in Table 5.

[36] Since the laser pulses are not emitted from the center of the telescope, the laser beam is not in view of the telescope for the first 300 m. When measurements starting near the surface are required, the emitter section and receiving telescope are tilted under various angles. Measurements from various elevation angles are combined into a profile, where elevations close to the horizontal yield NO_2 concentrations at low altitudes but pertaining to a certain horizontal extent away from the instrument (for a near-horizontal measurement, typically up to about 2500 m), while a zenith observation is performed exactly above the truck. Completing a vertical profile typically takes 50 minutes, providing data ranging in altitude from a few meters up to approximately 2500 m, with an accuracy of 0.2–0.4 $\mu g\ m^{-3}$. In Table 5 we list for each elevation angle the attainable altitude interval and best resolutions. The final altitude range obtained, and the corresponding accuracy, also depend on atmospheric conditions. Thus the vertical resolution of a profile varies, and typically is about 15 m at the lowest altitude, increasing to over 500 m at the highest altitude. The final resolution arises from averaging of data over an altitude range, based on signal-to-noise considerations.

[37] In addition to profile measurements, we used the lidar to investigate spatial and temporal changes in the horizontal NO_2 field. In this alternative operational mode, the lidar instrument measures at a fixed elevation angle of 12 degrees. Spatial inhomogeneities in the NO_2 concentrations are studied by alternating the azimuth direction of the laser pulse every 3.8 s during approximately half an hour. In this way, the lidar nearly simultaneously measures NO_2 concentrations of two volumes of air at the same altitude but approximately 2 km apart. Temporal homogeneities are investigated by measuring in one azimuth direction for about half an hour and determining averages over a few minutes in time. We find that spatial and temporal changes in NO_2 concentrations observed are commonly of the order of 10–20% and occasionally up to 40–50%.

3.3. In Situ NO_2 Monitors

[38] The in situ NO_2 monitor at ground level at Cabauw is part of monitoring activities in the framework of the RIVM Dutch National Air Quality Monitoring Network (LML, see www.rivm.nl/lml). The site at Cabauw is one of 45 sites in the Netherlands where nitrogen oxides are monitored on a continuous basis with one minute intervals, using automatic analyzers based on chemoluminescence (Thermo Electron 42W). The measuring range of the monitor is 0–1915 $\mu g\ NO_2\ m^{-3}$ and it has a detection limit of 1 $\mu g\ NO_2\ m^{-3}$ [*Van Elzakker*, 2001]. Owing to technical problems during the 2006 campaign no data were recorded before 5 September and from 7 to 10 September. In addition to the monitor at ground level, during the 2006 campaign a similar monitor was placed in the tower at Cabauw at a height of 200 m.

3.4. Sun Photometer Instruments

[39] At the Cabauw site, there are two operational photometers that routinely measure the aerosol optical thickness (AOT). The first is a CIMEL Electronique 318A spectral radiometer that is part of the Aerosol Robotic Network (AERONET) [see *Holben et al.*, 1998]. The second is an SPUV-6 instrument [*Stammes and Henzing*, 2000; *Knap et al.*, 2003], manufactured by Yankee Environmental Systems. The SPUV AOT values are calculated according to the methods described by *Ingold et al.* [2001]. On a number of days during the 2006 DANDELIONS campaign, the operational instruments were augmented by a small hand-held photometer (GLOBE instrument RGK-530) that is used as part of the Global Learning and Observations to Benefit the Environment (GLOBE) project [*Boersma and de Vroom*, 2006; *Brooks and Mims*, 2001]. For the CIMEL, AOT values are determined for wavelengths of 440, 675, 870, and 1020 nm; for the SPUV, 368, 501, 675, 780, and 871 nm; and for the hand-held photometer, 508 and 625 nm. The SPUV is sampled every second and 1-minute statistics

are stored. Intervals for the other instruments vary, with values on the order of several minutes. The SPUV and CIMEL measurements were screened for the presence of clouds using triplet variability.

[40] In addition to AOT, AERONET provides aerosol optical and physical properties such as refractive index and particle number size distribution (see http://aeronet.gsfc.nasa.gov/index.html). The AERONET data are also available for the 2005 campaign.

3.5. Pandora

[41] The spectrometer Pandora-1 from Goddard Space Flight Center participated during the second half of the DANDELIONS-2 campaign. Pandora-1 measures direct-sun irradiances from 270 to 500 nm at a resolution of about 0.5 nm. The outdoor head sensor was mounted on a tracking system and held a single strand fiber optics cable, which collected the light passed through a collimator (1.6° FWHM field of view) and a filterwheel. The other end of the fiber was inside and connected to a 75 mm focal length spectrometer using a 1024 × 1 pixel CMOS detector, stabilized to room temperature. The whole system weighs less than 15 kg. The total NO_2 column is retrieved using the DOAS method in the 400 to 440 nm window using a fixed reference spectrum. To estimate the NO_2 amount in the reference spectrum, a bootstrap method as described by *Cede et al.* [2006] is applied. The Pandora instrument yielded only a limited amount of NO_2 results at the very end of DANDELIONS-2, owing to technical problems.

3.6. Additional Ground-Based Aerosol Data

[42] Additional aerosol data are obtained by instruments at Cabauw such as an optical particle counter equipped with a heated inlet providing spectra of volatile aerosol components, a Scanning Mobility Particle Sizer (SMPS, TSI Model 3321) and an Aerodynamic Particle Sizer Spectrometer (APS, TSI Model 3321) providing aerosol number size distributions in the range from 10 nm to 20 μm, a volatility meter, an aetholometer providing aerosol absorption, and an integrating nephelometer (TSI Model 3563) providing aerosol scatter at 450 nm (blue), 550 nm (green), and 700 nm (red). These instruments are fully specified at www.tsi.com. They provide in situ information on the aerosol physical and optical parameters at ground level. In well-mixed situations the ground level aerosol properties will be representative for the total boundary layer, if size distribution and refractive index are corrected for the temperature decrease with height and accompanying increase in relative humidity. This generally results in an increase of the extinction coefficient which could be observed with the boundary layer lidar (see section 3.8). From an evaluation of these effects the mixed layer AOT could be determined and from comparison with the satellite/CIMEL/SPUV-derived AOT the contribution of the mixed layer to the total AOT could be derived. Whether or not a well-mixed situation exists can be derived from the boundary layer lidar measurements and micrometeorological (heat flux) data at Cabauw.

3.7. Radiosondes

[43] We obtained pressure/temperature/humidity/wind speed/wind direction soundings from radiosondes launched from Cabauw. These were performed by soundings using Vaisala Radiosondes of type RS92-Kl, launched on meteorological helium filled balloons. Before sondes were launched, they were reconditioned and ground-checked, to remove contaminants from the sensor and recover the original sensor calibration. The system was completed by a DigiCORA III SPS311 (Sounding Processing Subsystem) Rawinsonde receiver.

[44] Pressure, temperature and humidity are measured at regular intervals (2 s) and transmitted to the surface by radio signals at a frequency of about 400 MHz. The speed and direction of wind was determined by means of the Loran-C navigation network. The sonde included a receiver module for this purpose.

[45] Radiosonde PTU performance is characterized by the following reproducibilities: pressure 0.5 hPa, temperature 0.2 K, humidity 2% RH. The F-thermocap temperature sensor has a fast response time; its time lag effect is negligible (less than 0.4 s at 1000 hPa, less than 2.5 s at 10 hPa). The solar insolation error is small (at 10 hPa, this was 0.5 K uncorrected, less than 0.1 K corrected). The U sensor reconditioning procedure minimizes any dry bias. The Barocap silicon pressure sensor is shock and fast temperature change resistant. The heated Humicap is a fast, defrosting humidity sensor.

3.8. Boundary Layer Lidar

[46] A continuously operating backscatter lidar ("boundary layer lidar" [cf. *Russchenberg et al.*, 2005]) at Cabauw provides data on boundary layer height, residual clouds and the performance of the cloud detection algorithm, as well as on the vertical distribution of the aerosol, the occurrence of detached layers and the representativeness of the satellite retrieved aerosol properties for those near the ground.

3.9. Additional Data

[47] In addition to the instruments described above, the routine instrumentation at the CESAR site also provides a wealth of information on clouds-aerosol-radiation measurements. These are potentially useful for validation and encompass instrumentation like standard meteorological instruments at different heights of the 200 m tower, backscatter lidars operating at different wavelengths and providing continuous information on boundary layer height and vertical aerosol distribution, two cloud radars that provide cloud heights and microphysics (the latter in combination with lidar), and aerosol in situ instruments (as described in section 1). Furthermore, the CESAR site contains a radiation station which is part of the Baseline Surface Radiation Network (BSRN). An overview of instrumentation, their products and the use of the suite of measurements at CESAR is described by *Russchenberg et al.* [2005] and at www.cesar-observatory.nl.

[48] At KNMI in De Bilt (52.10°N, 5.17°E) a Brewer instrument (Mark-III type) is operated routinely. Also, ozone sondes are launched weekly, with additional launches during the campaigns. The distance between Cabauw and De Bilt is about 35 km.

4. DANDELIONS Campaigns

[49] An overview of the instrumentation available during the campaigns is given in Table 2. Most of these instruments

measure on a continuous basis. Additional measurements by NO_2 lidar, radiosondes, ozone sondes and the GLOBE (Global Learning and Observations to Benefit the Environment) [cf. *Brooks and Mims*, 2001; *Boersma and de Vroom*, 2006] sun photometer were performed during days with forecasts for good weather. 'Golden days' are defined as days that have low cloud coverage during the satellite overpasses, and during which most of the instrumentation worked well. The golden days for intensive analysis in 2005 are 27 and 28 May and 19, 23, and 24 June, and in 2006 are 9, 10, 11, 12, 13, 20, 21, and 22 September. There are Aura overpasses over Cabauw once or twice per day; the average overpass time is 1.45 PM.

4.1. Satellite Data

[50] OMI operated flawlessly. The monthly spatial zoom mode, in which pixel sizes are 50% smaller in the across-track direction, was performed twice during the first campaign (unfortunately during overcast situations) and once during the second campaign (during good weather). For SCIAMACHY, during both campaigns an Operations Change Request was honored, maximizing the number of overpasses with nadir mode observations for Cabauw. In spite of some instrumental and platform downtime, on average, two overpasses per 3–4 days are available from SCIAMACHY.

[51] AOT over Cabauw is retrieved from OMI data for cloud-free pixels and the results are compared with those of the routine sun photometer measurements. Measurements with a GLOBE instrument were also taken during some days. The ground-based aerosol measurements may be used to validate the OMI AOT and to support assumptions made in the retrieval algorithm, namely the aerosol size distribution and composition, and if a series of data is considered, the accuracy of the retrieved AOT [cf. *Curier et al.*, 2008].

4.2. Ground-Based Aerosol Data

[52] Using the boundary layer lidar data, elevated aerosol layers may be detected and their influence on the AOT may be evaluated. We also intercompared results from different aerosol instruments, namely SPUV, CIMEL, GLOBE sun photometer, and OMI. We show that the ground-based instruments compare well, including those of the relatively simple GLOBE sun photometer which is used worldwide at high schools to provide aerosol optical thicknesses to a public database. Although the number of cloud-free days during the two campaigns is limited, and therefore the statistics are poor, we do draw some first conclusions on the quality of the OMI spectral aerosol optical thickness product.

4.3. Ground-Based NO_2 Data

[53] The quality of the NO_2 column retrieval can be studied for clear as well as partially cloudy conditions. In this paper, most conclusions on NO_2 result from data with cloud fractions up to about 20%. The MAX-DOAS instruments pointing in different directions provide information about the spatial variability. We quantify this by calculating a heterogeneity index from observations in three different azimuth directions by the Heidelberg MAX-DOAS. MAX-DOAS instruments at different altitudes provide insight in the vertical distribution. These data are not used in the current paper, but will be explored in the future. An in situ NO_2 monitor at ground level is available permanently at Cabauw as part of the national network (LML) for air pollution monitoring. A second monitor was placed at the tower, at 200 m altitude, during the September 2006 campaign. These in situ data are compared with lidar NO_2 observations.

[54] Then, the results of the various instruments measuring NO_2 are intercompared. Lower tropospheric profiles (0–2.5 km) were measured by NO_2 lidar during the 2006 campaign.

[55] In the next section, we present some of the measurements, show that they compare well with in situ measurements, and indicate the variability in the NO_2 profile during the 2006 campaign. We also present intercomparisons between the ground-based DOAS results and OMI and SCIAMACHY measurements of NO_2 from space.

5. Results

5.1. Comparison of MAX-DOAS and in Situ NO_2 Observations

[56] To demonstrate the quality of the MAX-DOAS observations, a comparison with an independent NO_2 measurement, in this case taken by the in situ monitor, is required. MAX-DOAS provides tropospheric vertical column densities, whereas the in situ monitor measures surface concentrations. Assuming the tropospheric NO_2 profile shape does not change, the two measured quantities are strongly correlated. In Figure 1, actual correlations are shown between the Bremen MAX-DOAS and the in situ monitor during two weeks in the 2005 campaign. With a few exceptions, the NO_2 measurements from both instruments appear to be well-correlated. The correlation coefficient is 0.63. This is promising considering that the in situ monitor takes point measurements while the MAX-DOAS measurements are sensitive to a wider field both horizontally and vertically. In addition, there was a 200 m distance between the Bremen MAX-DOAS and the in situ NO_2 monitor.

[57] More accurate comparisons could be made if the profiling capability of the MAX-DOAS [*Wittrock*, 2006] was exploited. The lowest point in the NO_2 profile would then be compared with the surface concentrations. Preliminary results (not shown) are satisfactory, but more work needs to be done on the MAX-DOAS profile retrievals.

5.2. Intercomparisons of MAX-DOAS NO_2 Observations

[58] MAX-DOAS NO_2 observations were made almost continuously throughout the two campaigns. Good agreement between the data from the three ground-based MAX-DOAS instruments is obtained. An example from the 2005 campaign is shown in Figure 2, which includes also the OMI-L2 and SCIAMACHY (TEMIS product) overpass data. Data shown are based on the 3° elevation angle observations. We found that 1° elevation angle results probably suffered from obstructions in the optical path, and therefore 3° is the lowest angle that all instruments share. As explained in section 3.1.1, the lowest elevation angles yield the highest tropospheric sensitivity, and are thus used for retrieval of tropospheric NO_2.

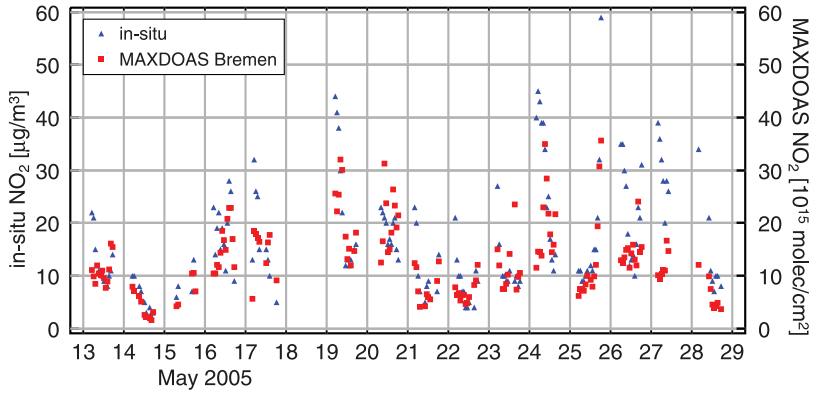

Figure 1. Comparison between NO_2 surface concentrations from the in situ data and NO_2 tropospheric vertical columns from the Bremen MAX-DOAS instrument (using the fitting window in the VIS) for part of the 2005 campaign. MAX-DOAS measurements have been interpolated to the in situ measurement times; only collocations within 1 h are taken into account. The correlation coefficient is 0.63.

[59] The gaps in the time series of ground-based measurements result from the application of the selection criterion based on the comparison of the NO_2 columns retrieved from 15° and 30° of elevation discussed above.

[60] The level of agreement achieved between the MAX-DOAS instruments is quantitatively summarized in correlation plots (Figure 3) where tropospheric NO_2 columns from the BIRA instrument are compared to those from the other groups, for the 2005 campaign. Very good agreement is found between the BIRA and Bremen data sets (Pearson correlation coefficients [*Pearson*, 1896; *Rodgers and Nicewander*, 1988] of 0.9 and slope of 1.1), and also between BIRA and the three Heidelberg telescopes (correlations between 0.82 and 0.91), especially considering that the BIRA instrument was 200 m away from the other two instruments.

[61] After further homogenization of the BIRA and Heidelberg data sets regarding the NO_2 absorption cross sections considered for the retrieval, an even better agreement is found, reaching a correlation coefficient of 0.91 and a slope of 0.99. This level of agreement is only achieved when considering the southwest-pointing Heidelberg telescope: this is approximately in the same direction as the two other instruments. This highlights the importance of horizontal

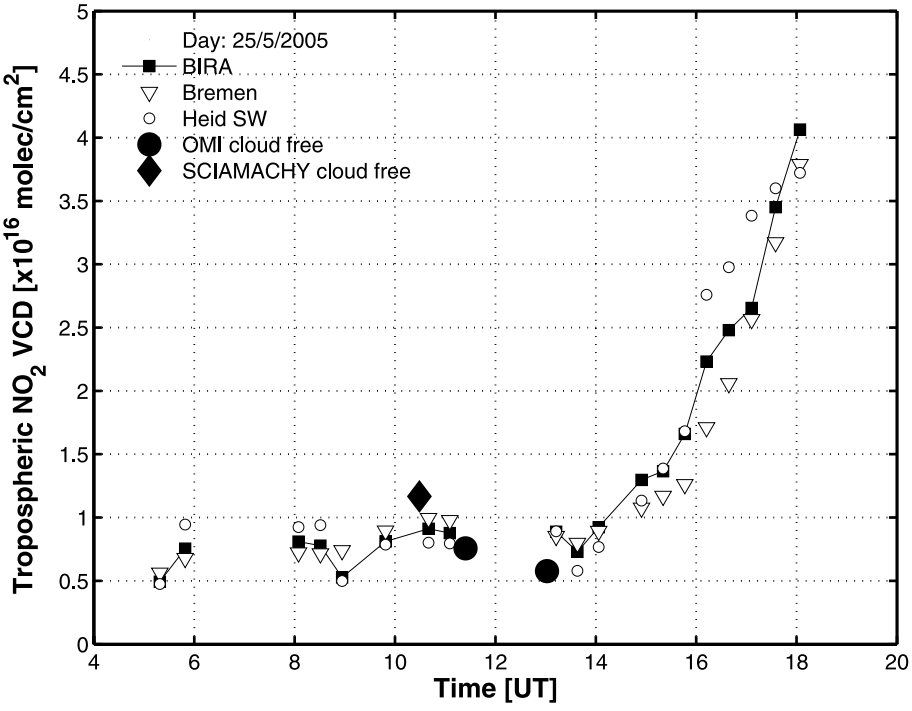

Figure 2. Comparison of collocated ground-based MAX-DOAS and satellite measurements on 25 May 2005. Tropospheric NO_2 vertical columns (VCD) are retrieved using the geometrical approximation, using also the selection criterion that 15 and 30 degree observations must be consistent; OMI (Level 2 product) and SCIAMACHY (TEMIS product) data are retrieved within 200 km radius around Cabauw under cloud-free conditions (cloud fractions less than 20%).

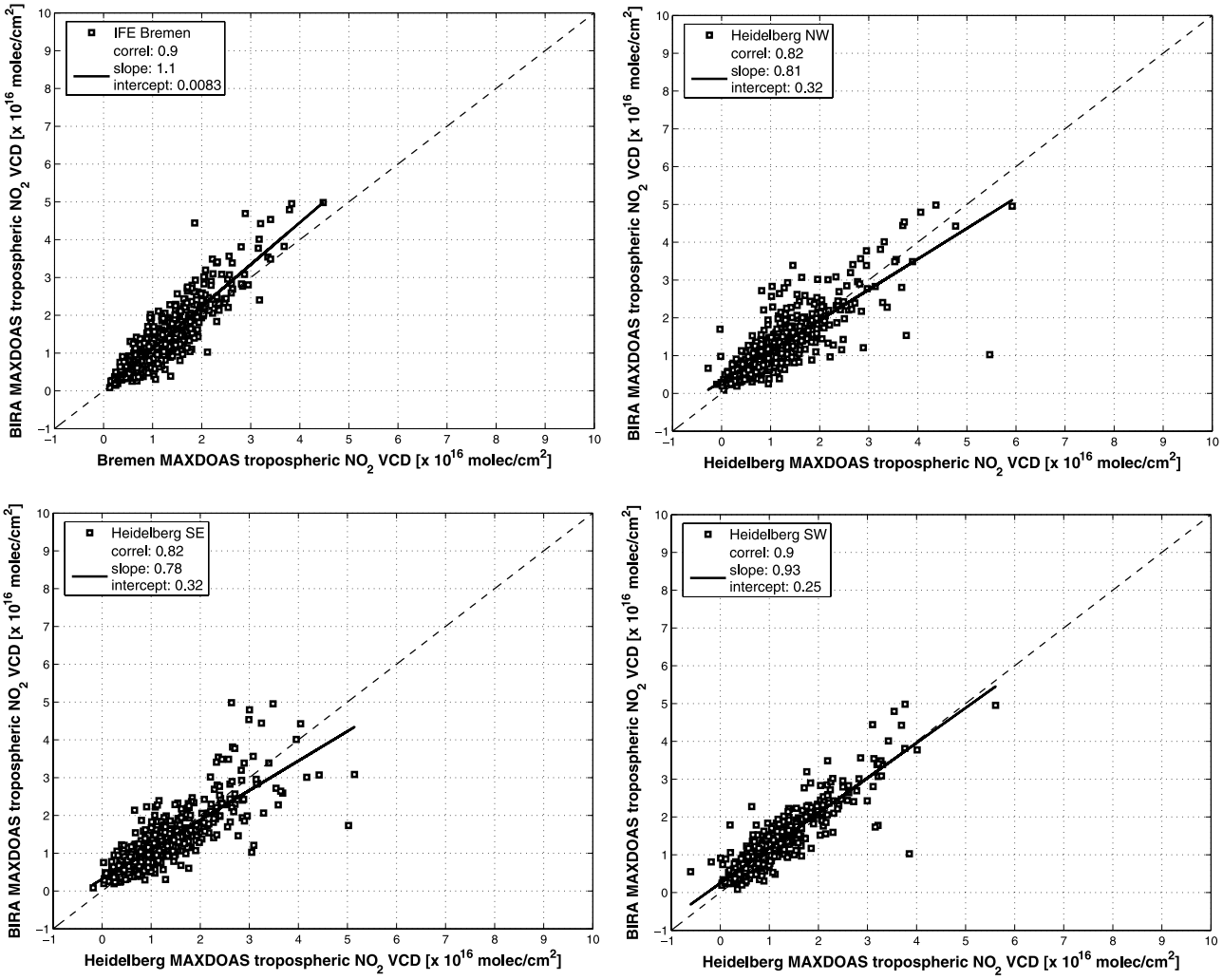

Figure 3. Scatterplots of the tropospheric NO_2 columns retrieved during the 2005 campaign from the BIRA MAX-DOAS instrument and (top left) the Bremen MAX-DOAS and the Heidelberg MAX-DOAS for the three pointing directions (top right) northwest, (bottom left) southeast, and (bottom right) southwest. The regression analysis parameters are given in the legends. It has to be noted that agreement with the Heidelberg observations can be further improved after homogenization of the retrieval settings (see text).

inhomogeneities in the NO_2 field that in some cases strongly affect the comparisons with satellite. The NO_2 field heterogeneity is discussed further in section 5.4; future campaigns will have to consider this aspect more specifically.

5.3. MAX-DOAS and Satellite Comparison

[62] The different MAX-DOAS data sets have been compared to the OMI-L2 and OMI-L4 cloud-free data (O_2–O_2 cloud fractions in the OMI products below 20%) for 2005. In order to produce the correlation plots presented in Figure 4, the MAX-DOAS data have been linearly interpolated to the satellite overpass time. The corresponding regression analysis parameters are given in Table 6.

[63] For the two OMI algorithms, the vertical columns were generally distributed in values ranging from 0 to about 2.5×10^{16} molec cm^{-2}. In one case the ground-based MAX-DOAS column significantly exceeded the corresponding satellite values (ground-based value equaled 3×10^{16} molec cm^{-2}), possibly owing to a local enhancement of the NO_2 concentration at Cabauw. A second outlier (reported between parentheses in Figure 4) can be observed in the OMI level 4 products. In this outlier case, the reported NO_2 column was twice as large as the corresponding value in the OMI-L2 product. The point has been excluded from the regression analysis. The larger tropospheric NO_2 column obtained may point to a difference in the assumption of NO_2 under the clouds (“ghost column”) between the two algorithms, since the cloud fraction was rather large, 18%.

[64] The regression analyses show that similar results were achieved with the BIRA and the Bremen data sets, the correlation coefficient between ground-based and satellite data being about 0.6 for OMI-L2 and about 0.5 for OMI-L4. A lower correlation was obtained with the Heidelberg data when considering only the SW direction (closest to the viewing direction of both Bremen and BIRA instruments), possibly due to the smaller number of coincidences with this instrument, and also the shorter integration time used which may increase the sensitivity to local inhomogeneities

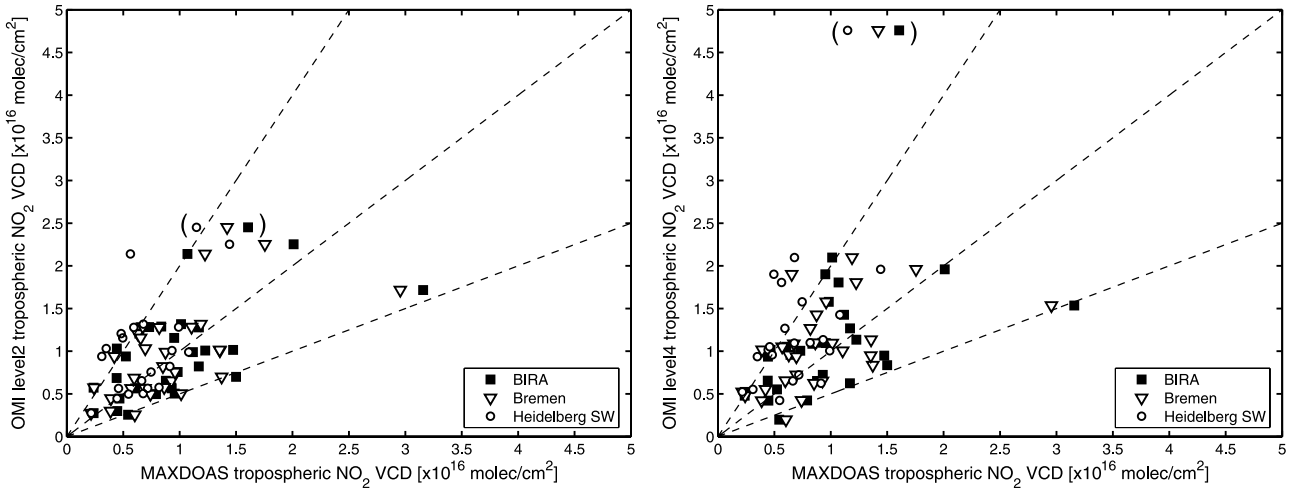

Figure 4. Correlations between tropospheric NO_2 from the three MAX-DOAS instruments at Cabauw (BIRA, Bremen, and Heidelberg SW direction) and (left) OMI-L2 or (right) OMI L4. OMI data are included if cloud fractions were less than 20%. Correlation and regression coefficients are summarized in Table 6.

in the NO_2 field. In order to further explore the impact of possible horizontal smoothing effects on the comparison results, the Heidelberg measurements simultaneously recorded from all three directions have been averaged and again compared with satellite data. The resulting correlation coefficients, also given in Table 6, have significantly improved and are now the highest of the three MAX-DOAS instruments. This suggests that the scatter in MAX-DOAS versus satellite comparisons is, indeed, largely dominated by spatial (and temporal) averaging effects.

[66] As is evident from the regression results, the OMI tropospheric NO_2 columns seem to be systematically lower than the MAX-DOAS results, for both OMI products considered. However, it must be noted that the correlation coefficients are rather poor in all cases, which might be due to several reasons including uncertainties in both ground-based (geometrical approximation) and satellite retrievals (AMF sensitivity to errors in aerosols, clouds and NO_2 profile shape). As already mentioned, the main reason for the poor correlation is probably related to the spatial mismatch between the ground-based MAX-DOAS observation (essentially local) and the satellite measurements (averaged over the OMI footprint). One expects that the collection of more comparison points will help in improving the statistical significance of the comparisons. Hence further studies will be conducted bringing in measurement data from the second DANDELIONS campaign. This and detailed validation of the satellite retrievals during the campaigns is the topic of future work, in which also different algorithm results, strength of collocation criteria, role of ghost columns, and for OMI, also swath angle dependence should be considered.

[67] The direct-sun DOAS and Pandora results were analyzed and compared with OMI-L2 and OMI-L4 total NO_2. Note that direct-sun air masses are simply the geometric airmass factor. Direct comparisons with OMI-L2 are presented in Figure 5, where the top panel shows the DOAS and Pandora direct-sun observations from 6 through 22 September 2006, with the OMI-L2 total NO_2 overplotted, and Figure 5 (bottom) shows the correlation between collocated direct-sun and OMI-L2 (Figure 5, bottom left) and OMI-L4 (Figure 5, bottom right) total NO_2. Pearson correlation coefficients are 0.68 (OMI-L2) and 0.66 (OMI-L4); for details see Table 7. Correlations are computed taking into account only those observations where both OMI-L2 and OMI-L4 had valid results.

5.4. Investigations of NO_2 Spatial Heterogeneity

[68] Assuming that the tropospheric NO_2 layer is horizontally homogenous, the observed NO_2 SCDs for the different azimuth angles observed from the three telescopes of the Heidelberg instrument should have been similar. In turn, from the observed differences for the various viewing directions, the horizontal heterogeneity of the NO_2 concentration field can be estimated. Such an estimation is very important for the validation of satellite instruments with ground-based observations. In cases of strong horizontal gradients, ground-based observations may not be representative for the average value within a satellite ground pixel.

Table 6. Statistical Analysis of Comparisons Between Tropospheric NO_2 From MAX-DOAS Data and OMI (L2 and L4)[a]

	N	C	I	Slope	rms	rms2
			BIRA South			
OMIL2	29	0.6	4.29	0.52	4.82	52%
OMIL4	29	0.51	6.16	0.44	5.35	52%
			Bremen Southwest			
OMIL2	29	0.63	3.93	0.59	4.44	48%
OMIL4	29	0.52	5.99	0.48	5.18	50%
			Heidelberg Southwest			
OMIL2	21	0.45	4.27	0.8	5.38	56%
OMIL4	21	0.39	6.84	0.67	6.50	57%
			Heidelberg Spatial Average			
OMIL2	21	0.65	1.99	0.85	3.89	40%
OMIL4	21	0.57	4.89	0.71	4.74	42%

[a]N denotes number of collocations, C is Pearson correlation coefficient, I is intercept in units of 10^{15} m^{-2}, slope denotes result of linear regression analysis, rms denotes rms difference of ground-based - OMI in units of 10^{15} m^{-2}, and rms2 denotes the same in percent relative to the average OMI value.

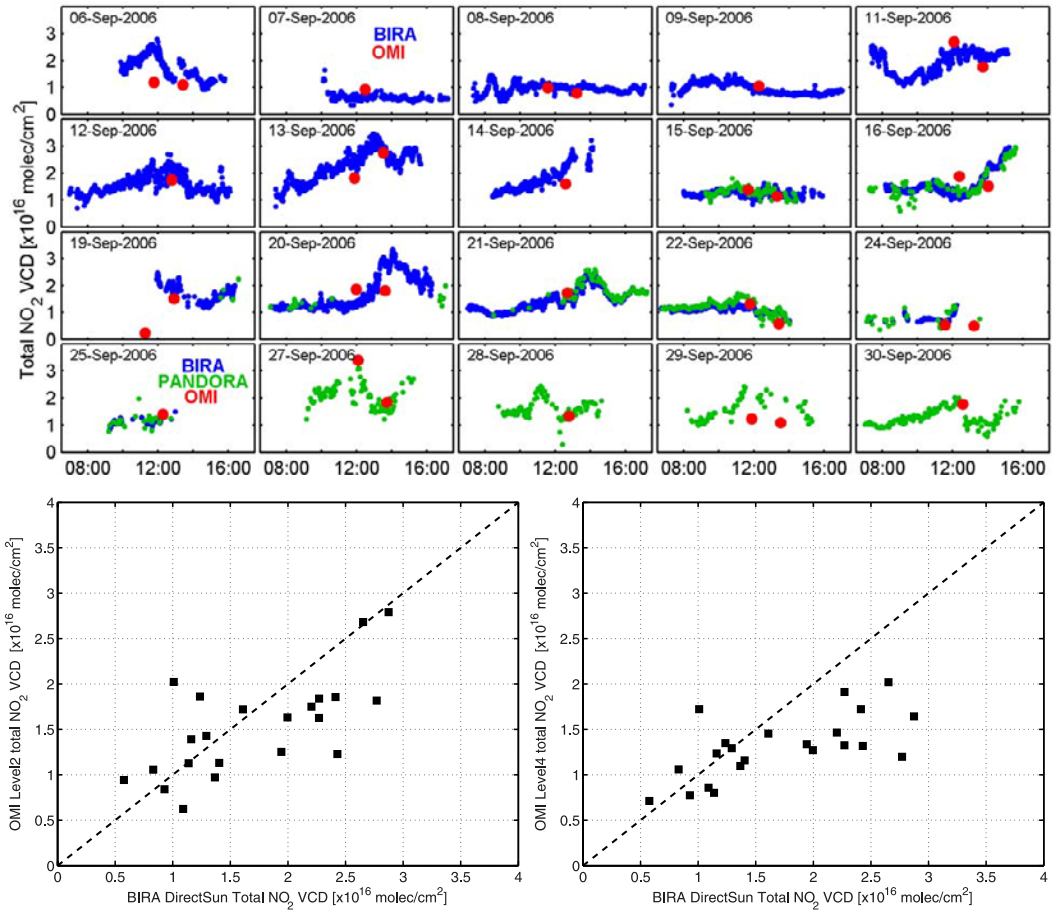

Figure 5. (top) All direct-sun tropospheric NO_2 observations, with OMI tropospheric NO_2 during clear days overplotted. (bottom) Correlations between NO_2 from (left) OMI-L2 and (right) OMI-L4 and the most closely collocated observation by the BIRA direct-sun instrument. See Table 7 for correlation statistics.

[69] Since the horizontal extension of the absorption paths along the line of sight is largest for low telescope elevation, we used the observations at the lowest elevation angles that had an unobstructed path, namely those at 3°, for the estimation of the heterogeneity of the tropospheric NO_2 concentration field. We did this by evaluating the SCD in the three azimuthal viewing directions at 3°, and calculating the ratio of the maximum and the minimum. A horizontally homogenous concentration field yields a ratio of one; the more this ratio deviated from unity, the larger were the horizontal gradients. In addition to the strength of the horizontal gradients, also information on the direction of the NO_2 gradient was derived. Since the Heidelberg MAX-DOAS was limited to three viewing azimuth directions, limited information on the direction of the horizontal gradients was derived. This information indicated that in future applications, it will be interesting to measure at many more azimuthal angles. The results are shown in Figure 6, which displays the time series of the ratios at daily noon. High ratios indicate strong gradients; the color of the points indicates the direction of the gradient (direction toward higher values).

[70] For the interpretation of the retrieved information on the gradient of the tropospheric NO_2 concentration field, it is important to consider two effects which can affect the observed SCDs, especially for low elevation angles: first, the sensitivity on the relative azimuth angle (between the telescope and the sun). This dependency becomes more pronounced for increasing solar zenith angle (SZA) and increasing aerosol load [*Wagner et al.*, 2004]. Second, we must consider the effect of the atmospheric aerosol load on the atmospheric visibility and thus on the horizontal extension of the absorption paths along the line of sight. Thus, depending on the aerosol load, the calculated ratio represents information on gradients over areas of different horizontal extension. We estimated the magnitude of both effects by means of radiative transfer calculations using the radiative transfer model TRACY-II [*Deutschmann and Wagner*, 2006; *Wagner et al.*, 2007]. The dependence on the azimuth angle was found to be generally very small. For a pure Rayleigh atmosphere and various aerosol loads

Table 7. Statistical Analysis of Comparisons Between Total NO_2 From BIRA Direct-Sun Data and OMI (L2 and L4)[a]

	N	C	I	Slope	rms	rms2
OMI-L2	22	0.68	6.08	0.54	5.32	35%
OMI-L4	22	0.66	7.39	0.33	6.57	50%

[a]Conventions as in Table 6.

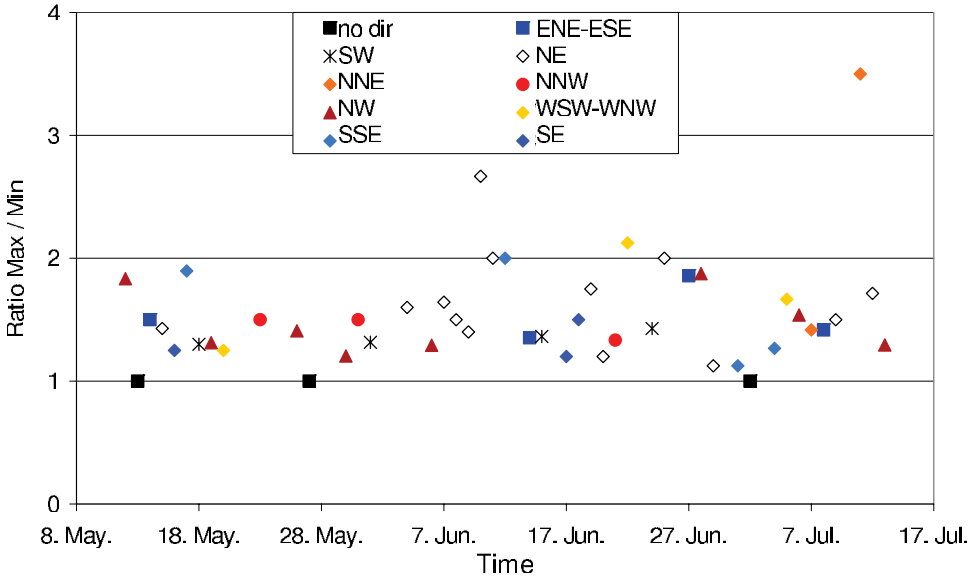

Figure 6. Maximum and minimum NO_2 SCD observed for an elevation angle of 3° of the Heidelberg MAX-DOAS telescopes observing under three different azimuth angles at Cabauw during the DANDELION campaign in 2005. High ratios indicate large horizontal gradients of the tropospheric NO_2 concentration field; colors indicate the direction of the gradient (directed toward higher values).

(optical thickness 0.1–1) the variation was typically below 15% (for SZA ranging from 20° to 80°). Thus, almost all observed ratios of the maximum and minimum NO_2 SCDs (see Figure 6) were much larger than what could be explained by this azimuth dependence. In contrast, the effect of aerosol scattering on the horizontal extension, for which the calculated ratio is representative, can be very large. Assuming a layer height of 1 km, the geometrical path length inside this layer for an elevation angle of 3° is about 19 km. For a pure Rayleigh atmosphere the molecular scattering reduces this path length to an effective path length of about 17 km. For additional aerosol scattering the path length decreases further. Assuming an optical thickness of 0.1 (0.3, 1.0) in a layer between the surface and 1 km altitude, the effective path length is only about 12 km (8 km, 4.5 km). Thus for typical aerosol optical

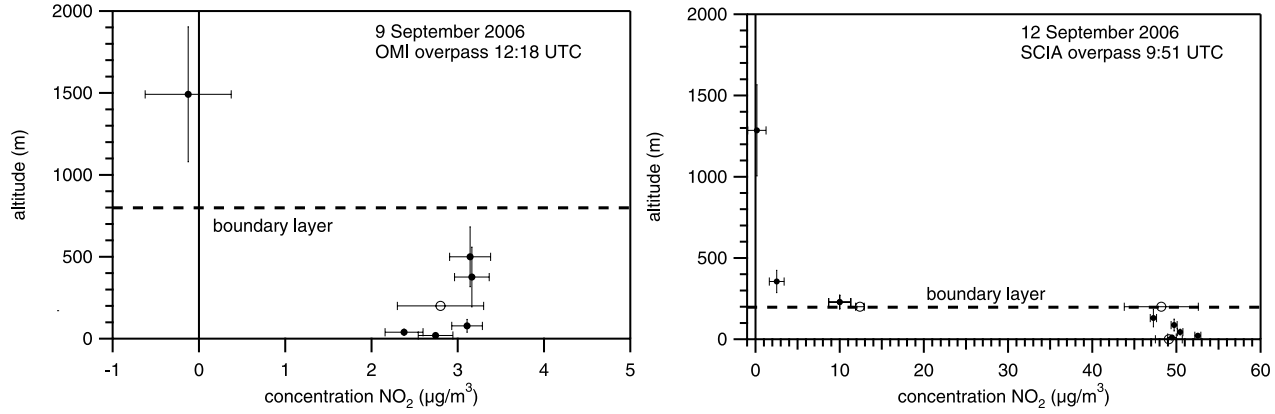

Figure 7. Lidar NO_2 profile (black circles) and NO_2 monitor value (open circle) measured at Cabauw. Horizontal bars indicate two-sigma values for the concentration. For the lidar data, vertical bars indicate the height intervals over which concentrations have been determined. The boundary layer height is indicated by a dashed line. (left) Clean day, 9 September 2006 (lidar measurement from 1204 to 1252 UT). On this day, the NO_2 monitor at ground level was not operational. NO_2 monitor data at 200 m were averaged over the lidar integration time. (right) Polluted day, 12 September 2006 (lidar measurement from 0937 to 1026 UT). For the NO_2 monitor data at ground level an average was made for the time the monitor was operational during this interval, from 1003 to 1017 UT. For the data of the NO_2 monitor at 200 m two averages were determined; the lower average, for 0937 to 1017 UT, is for the situation that the NO_2 monitor is above the boundary layer; the higher value, for 1017 to 1026 UT, is for the situation that the NO_2 monitor is situated below the boundary layer.

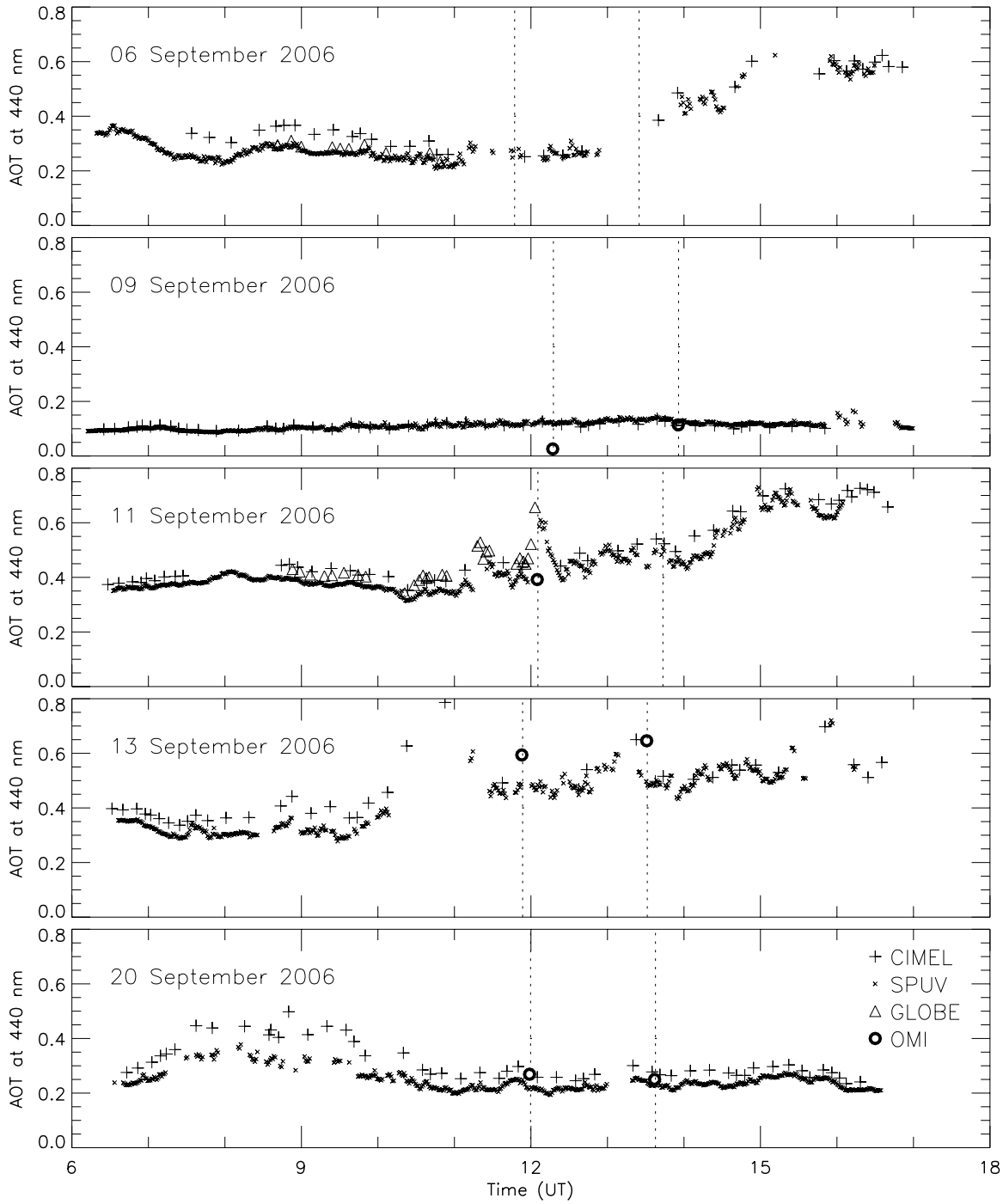

Figure 8. Time series of ground-based aerosol measurements at Cabauw. Shown are aerosol optical thicknesses (AOT) at 440 nm from SPUV (crosses), CIMEL (pluses), and hand-held GLOBE sun photometer (triangles, only on 6 and 11 September 2006). Overplotted are vertical lines indicating Aura overpass times, and circles indicating measured OMI AOT values. For SPUV and GLOBE, AOT values at 440 nm are found by interpolation and extrapolation as described in the text.

thicknesses the horizontal extension, for which the calculated ratio is representative, ranges between about 10 and 25 km. In principle, the visibility of the atmosphere can be estimated from the O_2-O_2 absorption retrieved from the spectra [*Wagner et al.*, 2004]. However, such a detailed analysis is beyond the scope of this study.

[71] The impact of the spatial variability is also visible in Figure 3, which was discussed in section 5.2.

5.5. Comparison of NO_2 Lidar With in Situ Data

[72] On golden days, i.e., days with low cloud coverage, during September 2006 lidar NO_2 profiles were measured at

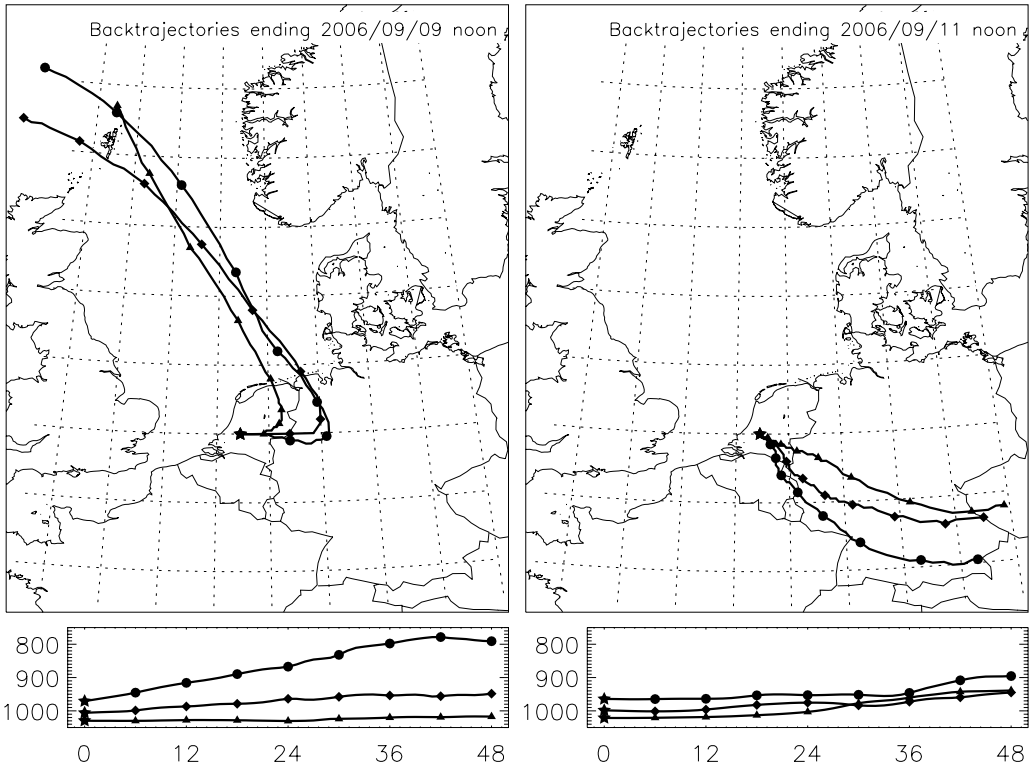

Figure 9. (top) TRAJKS back-trajectories, indicating the origin of the air masses observed during two 'golden days' in September 2006: (left) 9 September and (right) 11 September. Stars indicate the endpoint of the trajectories; other marks along the trajectories are spaced 6 h apart. (bottom) Pressures in hPa as functions of the time in hours before the end of the trajectory.

Cabauw (51.9°N, 4.9°E). Profile measurements take about 50 minutes and are timed to coincide with a SCIAMACHY or OMI overpass. In Figure 7, examples are shown of profile measurements for a relatively clean day, 9 September 2006, and for a polluted day, 12 September 2006. These measurements illustrate the general observation that the concentration of NO_2 is higher at ground level and drops to below the detection limit within the accuracy of the measurement above the boundary layer. The boundary layer heights were provided by the boundary layer lidar at Cabauw and are indicated in Figure 7 by a dashed line. These figures show that the day-to-day variations in NO_2 at the surface may be considerable, from around 3 μg NO_2 m^{-3} on a clean day to more than 50 μg NO_2 m^{-3} on a polluted day. Also, large diurnal variations may occur (not shown). The open symbols in Figure 7 correspond to in situ NO_2 monitor data. For 9 September only data of the NO_2 monitor located at 200 m were obtained. The NO_2 monitor data are averaged over the 50 minutes that the lidar integrated. There is excellent agreement between the NO_2 monitor data point and the lidar-profile data point. On 12 September, excellent agreement between the lidar-derived NO_2 concentrations and the in situ data is observed. Around the SCIAMACHY overpass at 0951 UT, both the NO_2 monitor and the NO_2 lidar measured a high value of around 50 μg NO_2 m^{-3} at surface level. The value of the NO_2 monitor placed at 200 m rose from 10 to around 50 μg m^{-3} during the 50 minute lidar integration time. This is due to the boundary layer rising from below 200 m to higher altitudes during this period. We determined two averages for the NO_2 monitor data at 200 m; the lower value is for the situation that the NO_2 monitor is situated above the boundary layer and vice versa.

[73] A more detailed discussion of all profiles measured will be given by H. Volten et al. (manuscript in preparation, 2008).

5.6. Intercomparisons of Aerosol Optical Thickness Observations

[74] In Figure 8, time series of AOT at 440 nm derived with the four instruments are shown for some of the golden days during September 2006. The CIMEL AOT values are directly taken from level-1.5 files available from the AERONET network; for the other instruments, assumptions have been made. The SPUV measured the AOT at wavelengths of 368 and 501 nm, so in order to perform a sensible comparison, values at these wavelengths have been interpolated assuming a perfect Ångström law. A similar approach was followed to extrapolate GLOBE AOT values to 440 nm. Finally, the OMI multiwavelength aerosol product (OMAERO) reports AOT values at 442 nm. The wavelength difference with 440 nm is ignored.

[75] One striking feature from Figure 8 is the increase in AOT between 9 and 11 September. This happened at a time when the prevailing winds turned from north to southeast. This is consistent with back trajectories calculated with the TRAJKS model [*Scheele et al.*, 1996; *Stohl et al.*, 2001]. On 9 September (Figure 9, left), the back trajectories indicate

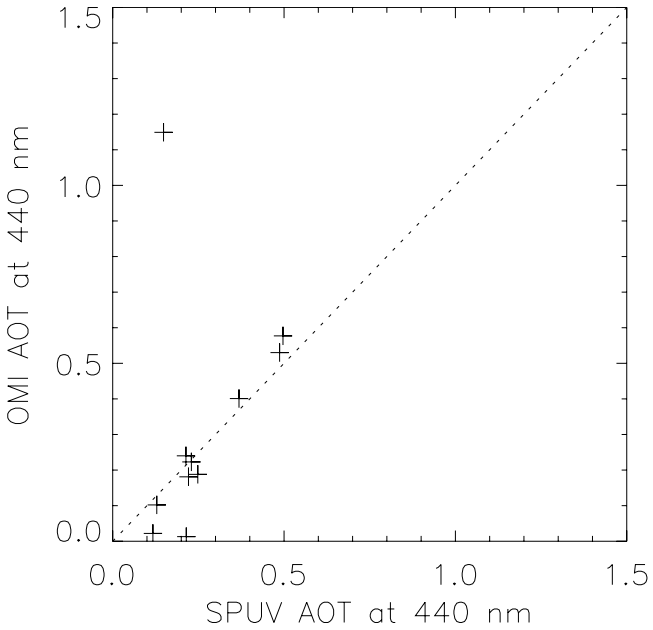

Figure 10. Scatterplot showing retrieved OMI AOT values compared with the SPUV AOT obtained closest in time to, and within 1.5 min of, the OMI overpass.

that a clean polar air mass was advected over the North Sea and then passed over a mostly rural area in northern Germany, while on 11 September (Figure 9, right), the trajectories were advected from Eastern Europe and passed over industrialized regions in Germany (especially the Ruhr Area). Note also that the symbols denoting 6-h intervals are closer together in the latter plot, indicating that wind speeds were low which allowed for the accumulation of industrial aerosols over the emission areas.

[76] The derived AOT exhibits similar trends for each of the three ground-based instruments throughout the golden days: almost every single rise and fall in AOT is seen in the results for each instrument. For 9 September, which was a particularly 'clean' day, the correspondence between the SPUV and CIMEL is nearly perfect. For the other days, the SPUV tends to underestimate the AOT with respect to the CIMEL. One possible cause is the interpolation based on the Ångström relation, although more sophisticated interpolations using additional, longer, wavelengths also used by the SPUV did not make a significant difference. Alternatively, the differences may be due to the fact that we used provisional level-1.5 AERONET data as opposed to quality-assured level-2 data. After the next CIMEL calibration has been performed and level-2 data are generated, new comparisons can be carried out and evaluated.

[77] The GLOBE handheld photometer may, owing to its limited pointing accuracy, easily be expected to perform less well than its more sophisticated counterparts. However, as the time series for 6 and 11 September show, the comparisons in fact hold up very well.

[78] Finally, the OMI-retrieved AOT values are very similar to those measured by the ground-based instruments at about the same times, apart from a couple of cases where OMI retrieved a near-zero AOT. Interestingly, very good comparisons are found despite OMI having a footprint of at least 13 $\times$ 24 km^2 while the photometers take point measurements. Additional comparisons for longer periods (providing more reliable statistics) and other AERONET stations are necessary for a proper assessment of the reliability of the OMI AOT.

[79] The favorable comparison between OMI and the ground-based instruments is further illustrated in Figure 10. Most of the points lie close to the 1:1 line. The point with high OMI AOT may be considered an outlier since we found it was obtained during a spell of varying cloud cover, and may therefore be cloud-contaminated. The correlation coefficient of the remaining ten points amounts to $r = 0.95$. Therefore we are quite confident in the OMAERO algorithm for areas like the Cabauw region, and, particularly, it gives us no reason to change the value of the surface albedo used for the Cabauw site in September. Effects of the surface albedo for May–July are discussed by *Curier et al.* [2008].

6. Conclusions and Future Work

[80] We present an extensive data set of ground-based and balloon sonde data on NO_2, aerosols, and ozone, which is available for validation of NO_2, aerosol, and ozone from satellite instruments, through the Aura Validation Data Center. We show that the data contain unique information on the spatial homogeneity and the vertical and temporal variability of NO_2. The homogeneity index presented indicates that on a number of days during the campaign, the NO_2 columns derived from measurements in different directions, varied significantly. This indicates that under polluted conditions, measurements in one single azimuth direction may not always be representative for the averaged field that the satellite observes.

[81] The first results of the RIVM NO_2 lidar, are presented. We show that concentrations near the surface and at 200 m compare well with in situ values at the same heights, which gives confidence that the overall lidar profiles, that range from the surface up to 2500 m, are reliable.

[82] NO_2 measurements from three MAX-DOAS instruments are compared and good agreement was found for similar viewing directions. Results from different viewing directions indicate significant horizontal inhomogeneities, a point that will have to be studied in more detail in future campaigns. A comparison between surface in situ data and MAX-DOAS tropospheric NO_2 columns shows good correlation, providing additional validation of the measurements. Tropospheric NO_2 data were compared to OMI-L2 and OMI-L4 NO_2 measurements, showing good agreement in light of the expected natural variability of NO_2, and the differences expected between average NO_2 concentrations in an extended (typically, 10 $\times$ 24 km or larger) OMI pixel and concentrations measured at the ground or in the vicinity of Cabauw. Total NO_2, from the BIRA direct-sun instrument and the Pandora instrument, compares favorably with OMI-L2 and L4.

[83] AOT values derived with the three ground-based instruments used compare favorably. Future plans include investigating the differences between SPUV and CIMEL AOT values at high aerosol loading, using longer time series. Furthermore, the correspondence between AOT values measured by the ground-based instruments with those retrieved

from OMI measurements are excellent, considering the difference in techniques, although it must be said that the statistics are quite poor. Comparisons between OMI and ground-based instruments will be extended to longer time series, as well as to other ground sites.

[84] **Acknowledgments.** We thank the support and research staff at KNMI, especially Jacques Warmer, for their role in helping to make the campaigns successful. We acknowledge Hans Bergwerff and René van der Hoff for measuring a number of NO_2 lidar profiles, Rinus Scheele for calculating the back-trajectories, Mark Kroon for technical support during both campaigns, and Manfred Gottwald for finding optimal SCIAMACHY operating conditions during both campaigns. In situ NO_2 monitor data, including a second monitor at 200 m during the second campaign, were kindly provided by the Dutch air quality monitoring network (LML). The Dutch-Finnish OMI instrument is part of the NASA EOS Aura satellite payload. The OMI project is managed by NIVR and KNMI in The Netherlands. We thank the OMI International Science Team for the satellite data used in this study. Part of this work was performed within the framework of the International ESA/KNMI/NIVR OMI "Announcement of Opportunity for Calibration and Validation of the Ozone Monitoring Instrument," providing early access to provisional OMI data sets and guidance to public OMI data. Provisional OMI NO_2 data, used for preliminary studies that are not published here, were obtained through AVDC. Publicly released OMI NO_2 data were obtained from the NASA Goddard Earth Sciences (GES) Data and Information Services Center (DISC), home of the GES Distributed Active Archive Center (DAAC). Part of the described research was funded by grants from the User Support Programme managed by the NWO-SRON Programme Bureau Space Research. OMI Research at KNMI is funded by NIVR. Travel by a number of the campaign participants was supported by ACCENT-Troposat. The Belgian contribution to OMI and SCIAMACHY validation was supported by the PRODEX CINAMON project.

References

Acarreta, J. R., J. F. de Haan, and P. Stammes (2004), Cloud pressure retrieval using the O_2–O_2 absorption band at 477 nm, *J. Geophys. Res.*, *109*, D05204, doi:10.1029/2003JD003915.

Berkhout, S., R. van der Hoff, D. P. J. Swart, and J. B. Bergwerff (2006), The RIVM mobile lidar—Design and operation of a versatile system for measuring atmospheric trace gases, in *Reviewed and Revised Papers of the 23rd International Laser Radar Conference (ILRC)*, edited by C. Nagasawa and N. Sugimoto, INDECO, Inc., Nara, Japan.

Blond, N., K. F. Boersma, H. J. Eskes, R. van der A, M. Van Roozendael, I. De Smedt, G. Bergametti, and R. Vautard (2006), Intercomparison of SCIAMACHY nitrogen dioxide observations, in-situ measurements and air quality modeling results over western Europe, *J. Geophys. Res.*, *112*, D10311, doi:10.1029/2006JD007277.

Boersma, K. F., and J. P. de Vroom (2006), Validation of MODIS aerosol observations over the Netherlands with GLOBE student measurements, *J. Geophys. Res.*, *111*, D20311, doi:10.1029/2006JD007172.

Boersma, K. F., E. Bucsela, E. Brinksma, and J. F. Gleason (2002), NO_2, in *OMI Algorithm Theoretical Basis Document*, vol. IV, *Trace Gas Algorithms*, edited by K. Chance, pp. 15–36, R. Neth. Meteorol. Inst., De Bilt, Netherlands.

Boersma, K. F., H. J. Eskes, and E. J. Brinksma (2004), Error analysis for tropospheric NO_2 retrieval from space, *J. Geophys. Res.*, *109*, D04311, doi:10.1029/2003JD003962.

Boersma, K. F., et al. (2006), Near-real time retrieval of tropospheric NO_2 from OMI, *Atmos. Chem. Phys. Discuss.*, *6*, 12,301–12,345.

Brooks, D. R., and F. M. Mims (2001), Development of an inexpensive handheld led-based Sun photometer for the GLOBE program, *J. Geophys. Res.*, *106*(D5), 4733–4740, doi:10.1029/2000JD900545.

Bucsela, E. J., E. A. Celarier, M. O. Wenig, J. F. Gleason, J. P. Veefkind, K. F. Booersma, and E. J. Brinksma (2006), Algorithm for NO_2 vertical column retrieval from the Ozone Monitoring Instrument, *IEEE Trans. Geosci. Remote Sens.*, *44*(5), 1245–1258, doi:10.1109/TGRS.2005.863715.

Cede, A., J. Herman, A. Richter, N. Krotkov, and J. Burrows (2006), Measurements of nitrogen dioxide total column amounts using a Brewer double spectrophotometer in direct-Sun mode, *J. Geophys. Res.*, *111*, D05304, doi:10.1029/2005JD006585.

Celarier, E. A., et al. (2008), Validation of Ozone Monitoring Instrument nitrogen dioxide columns, *J. Geophys. Res.*, *113*, D15S15, doi:10.1029/2007JD008908.

Curier, R. L., J. P. Veefkind, R. Braak, B. Veihelmann, O. Torres, and G. de Leeuw (2008), Retrieval of aerosol optical propertries from OMI radiances using a multi-wavelength algorithm: Application to western Europe, *J. Geophys. Res.*, doi:10.1029/2007JD008738, in press.

Deutschmann, T., and T. Wagner (2006), *TRACY-II Users manual*, Univ. of Heidelberg, Heidelberg, Germany.

Holben, B. N., et al. (1998), AERONET—A federated instrument network and data archive for aerosol characterization, *Remote Sens. Environ.*, *66*, 1–16.

Honninger, G., C. von Friedeburg, and U. Platt (2004), Multi axis differential optical absorption spectroscopy (MAX-DOAS), *Atmos. Chem. Phys.*, *4*, 231–254.

Ingold, T., C. Mätzler, N. Kämpfer, and A. Heimo (2001), Aerosol optical depth measurements by means of a Sun photometer network in Switzerland, *J. Geophys. Res.*, *106*(D21), 27,537–27,554, doi:10.1029/2000JD000088.

Knap, W. H., A. Los, W. Worrel, and P. Stammes (2003), Sunphotometry at the high altitude research station Jungfraujoch activity report 2003, technical report, Int. Found. High Alt. Res. Stn. Jungfraujoch and Gornergrat, Bern.

Koelemeijer, R. B. A., J. F. de Haan, and P. Stammes (2003), A database of spectral surface reflectivity in the range 335–772 nm derived from 5.5 years of GOME observations, *J. Geophys. Res.*, *108*(D2), 4070, doi:10.1029/2002JD002429.

Kurucz, R., I. Furenlid, J. Brault, and L. Testerman (1984), *National Solar Observatory Atlas 1: Solar Flux Atlas From 296 nm to 1300 nm*, 2nd ed., Natl. Sol. Obs., Sunspot, N. M.

Levelt, P. F., G. H. J. van den Oord, M. R. Dobber, A. Malkki, H. Visser, J. de Vries, P. Stammes, J. Lundell, and H. Saari (2006), The Ozone Monitoring Instrument, *IEEE Trans. Geosci. Remote Sens.*, *44*(5), 1,093–1,101, doi:10.1109/TGRS.2006.872333.

Noxon, J. F. (1975), Nitrogen dioxide in the stratosphere and troposphere measured by ground-based absorption spectroscopy, *Science*, *189*, 547–549.

Pearson, K. (1896), Mathematical contributions to the theory of evolution. III. Regression, heredity, and panmixia, *Philos. Trans. R. Soc., Ser. A*, *187*, 253–318.

Platt, U. (1994), *Differential Optical Absorption Spectroscopy (DOAS), Air Monitoring by Spectroscopic Techniques*, *Chem. Anal. Ser.*, vol. 127, John Wiley, Hoboken, N. J.

Richter, A., J. P. Burrows, H. Nüß, C. Granier, and U. Niemeier (2005), Increase in tropospheric nitrogen dioxide over China observed from space, *Nature*, *437*, 129–132, doi:10.1038/nature.04092.

Rodgers, J. L., and aW. A. Nicewander (1988), Thirteen ways to look at the correlation coefficient, *Am. Stat.*, *42*, 59–65.

Russchenberg, H., et al. (2005), Ground-based atmospheric remote sensing in The Netherlands: European outlook, *IEICE Trans. Commun.*, *E88-B*(6), 2,252–2,258, doi:10.1093/ietcom/e88-b.6.2252.

Scheele, M. P., P. C. Siegmund, and P. F. J. van Velthoven (1996), Sensitivity of trajectories to data resolution and its dependence on the starting point in or outside a tropopause fold, *Meteorol. Appl.*, *3*, 267–273.

Sinreich, R., U. Friess, T. Wagner, and U. Platt (2005), Multi axis differential optical absorption spectroscopy (MAX-DOAS) of gas and aerosol distributions, *Faraday Discuss.*, 153–164.

Stammes, P. (Ed.) (2002), *OMI Algorithm Theoretical Baseline Document*, vol. II, *Clouds, Aerosols and Surface UV Irradiance*, v2.0 ed., *aTBD-OMI-03*, NASA Goddard Space Flight Cent., Greenbelt, Md.

Stammes, P., and J. S. Henzing (2000), Multispectral aerosol optical thickness at De Bilt, 1997–1999, *J. Aerosol Sci.*, *31*, S283–S284.

Stohl, A., L. Haimberger, M. P. Scheele, and M. Wernli (2001), An intercomparison of results from three trajectory models, *Meteorol. Appl.*, *8*, 127–135, doi:10.1017/S1350482701002018.

Torres, O., R. Decae, P. Veefkind, and G. de Leeuw (2002), OMI aerosol retrieval algorithm, in *OMI Algorithm Theoretical Basis Document*, vol. III, *Clouds, Aerosols, and Surface UV Irradiance*, edited by P. Stammes, pp. 47–71, R. Neth. Meteorol. Inst., de Bilt, Netherlands.

Torres, O., A. Tanskanen, B. Veihelmann, C. Ahn, R. Braak, P. K. Bhartia, P. Veefkind, and P. Levelt (2007), Aerosols and surface UV products from Ozone Monitoring Instrument observations: An overview, *J. Geophys. Res.*, *112*, D24S47, doi:10.1029/2007JD008809.

van der A, R. J., D. H. M. U. Peters, H. Eskes, K. F. Boersma, M. Van Roozendael, I. De Smedt, and H. M. Kelder (2006), Detection of the trend and seasonal variation in tropospheric NO_2 over China, *J. Geophys. Res.*, *111*, D12317, doi:10.1029/2005JD006594.

Van Elzakker, B. (2001), Monitoring activities in the dutch national air quality monitoring network in 2000 and 2001, *Tech. Rep. 23101055*, Natl. Inst. of Public Health and the Environ., Bilthoven, Netherlands.

Wagner, T., B. Dix, C. v. Friedeburg, U. Frieß, S. Sanghavi, R. Sinreich, and U. Platt (2004), MAX-DOAS O4 measurements: A new technique to derive information on atmospheric aerosols: 1. Principles and information content, *J. Geophys. Res.*, *109*, D22205, doi:10.1029/2004JD004904.

Wagner, T., et al. (2007), Comparison of box-air-mass-factors and radiances for Multiple-Axis Differential Optical Absorption Spectroscopy (MAX-

DOAS) geometries calculated from different UV/visible radiative transfer models, *Atmos. Chem. Phys*, *7*, 1809–1833.

Wittrock, F. (2006), The retrieval of oxygenated volatile organic compounds by remote sensing techniques, dissertation, Univ. of Bremen, Bremen, Germany.

Wittrock, F., H. Oetjen, A. Richter, S. Fietkau, T. Medeke, A. Rozanov, and J. P. Burrows (2004), MAX-DOAS measurements of atmospheric trace gases in Ny-Ålesund—Radiative transfer studies and their application, *Atmos. Chem. Phys.*, *4*, 955–966.

M. Allaart, R. Braak, E. J. Brinksma, R. J. Dirksen, H. J. Eskes, W. H. Knap, P. F. Levelt, A. J. M. Piters, R. Rothe, J. P. Veefkind, and T. Vlemmix, Climate Research and Seismology Department, Royal Netherlands Meteorological Institute, PO Box 201, NL-3730 AE De Bilt, Netherlands. (brinksma@knmi.nl)

A. J. C. Berkhout, D. P. J. Swart, and H. Volten, LVM, RIVM, P.O. Box 1, NL-3720 BA, Bilthoven, Netherlands. (stijn.berkhout@rivm.nl; daan.swart@rivm.nl; hester.volten@rivm.nl)

A. Cede, NASA Goddard Space Flight Center, Greenbelt, MD 20770, USA.

E. A. Celarier, SGT, Inc., Greenbelt, MD 20770, USA. (edward.a.celarier.1@gsfc.nasa.gov)

R. L. Curier, G. de Leeuw, and M. Moerman, TNO Defense, Security and Safety, Postbus 96864, NL-2509 JG Den Haag, Netherlands. (lyana.curier@tno.nl; gerrit.deleeuw@tno.nl)

C. Fayt, C. Hermans, G. Pinardi, and M. van Roozendael, Belgian Institute for Space Aeronomy, 3 Avenue Circulaire, Brussels B-1180, Belgium.

O. W. Ibrahim, Institute for Environmental Physics, Heidelberg University, Im Neuenheimer Feld 229, D-69120 Heidelberg, Germany.

H. Oetjen, A. Richter, A. Schönhardt, and F. Wittrock, Institute of Environmental Physics, University of Bremen, Postfach 33 04 40, D-28334 Bremen, Germany.

T. Wagner, Max-Planck-Institute for Chemistry, Postfach 3060, D-55020 Mainz, Germany.